Low-Energy Electron and Low-Energy Positron Holography

S. Y. Tong, H. Huang, and X. Q. Guo

Laboratory for Surface Studies and Department of Physics, University of Wisconsin–Milwaukee, Milwaukee, Wisconsin 53201

(Received 11 June 1992)

We demonstrate holographic reconstruction using low-energy electron-diffraction (LEED) and low-energy positron-diffraction (LEPD) intensity spectra. Calculated LEED and LEPD intensity spectra from a multiple-scattering method are inverted to produce high-fidelity images of near-neighbor atoms whose positions are measured from an adatom. We show that low-energy positron diffraction is better suited for holographic reconstruction because positron scattering in solids is weaker than that of electrons.

PACS numbers: 68.35.Bs, 61.14.Hg, 61.16.–d, 68.55.–a

There is considerable interest in the development of local electron holography in which an adsorbate atom or impurity atom acts as a beam splitter for either emitted electrons [1–3] or scattered electrons [4,5]. Multiple-energy phase-summing methods were introduced to eliminate image artifacts produced by multiple scattering [6–8]. While such multiple-energy methods produced essentially artifact-free three-dimensional atom images [5–8], they required a considerable database in (θ,ϕ,k) space, thus putting a major burden on data acquisition. In this Letter, we indicate that positron diffraction is better suited than electron diffraction for holographic reconstruction because of the positron's weak scattering and large damping in solids. It is apparent that positrons are close to being the ideal particles for three-dimensional image reconstruction because these particles embody the advantages of both photons (weak elastic scattering) and electrons (high surface sensitivity via a large inelastic damping). We illustrate these observations by inverting low-energy electron-diffraction (LEED) and low-energy positron-diffraction (LEPD) intensity-voltage spectra calculated from identical multiple-scattering methods [9,10], using the respective phase shifts and inelastic dampings for electrons and positrons. We show that for positron holography, multiple-scattering artifacts are rapidly eliminated and high-fidelity atom images emerge after summing over only a few energies. Inversion of LEED spectra was attempted in the 1970's [11], but the attempt failed because it involved Fourier transforming integral-order I-V spectra. In this paper, we present a data inversion method for fractional-order I-V spectra based on the holographic principle.

The first observation of LEPD was made by Rosenberg, Weiss, and Canter in 1980 [12]. This discovery was followed by an experimental advancement in which the concept of "brightness enhancement" was introduced [13]. The theoretical analysis of LEPD spectra was made easy by the ready availability of multiple-scattering methods developed earlier for LEED. The early works of LEPD [14,15] pointed out an important difference between LEPD and LEED: In LEPD, the scattering potential between the positron and the atomic nucleus is repulsive because they have the same sign. This repulsive interaction has significant consequences [16,17], the most important of which is the considerably weaker positron-atom elastic scattering. Classically, a repulsive Coulomb potential keeps a positron at distances larger than the turning point $R_t = Ze^2/E_p$, where E_p is the kinetic energy of the positron. By contrast, an attractive potential allows an electron to have considerable lifetime at distances $r \le R_t$. The different pictures are shown schematically in Fig. 1. The weaker positron-atom scattering can also be seen by comparing the exact scattering factor given by

$$f(\mathbf{k}_i,\mathbf{k}_f) = -\frac{m}{2\pi\hbar^2}\int e^{-i\mathbf{k}_f\cdot\mathbf{r}_1}\left[v(\mathbf{r}_1)\delta(\mathbf{r}_1,\mathbf{r}_2)+\frac{2m}{\hbar^2}v(\mathbf{r}_1)G(\mathbf{r}_1,\mathbf{r}_2)v(\mathbf{r}_2)+\cdots\right]e^{i\mathbf{k}_i\cdot\mathbf{r}_2}d\mathbf{r}_1\,d\mathbf{r}_2 \quad (1)$$

with the single-scattering (Born approximation) form

$$f_B(\mathbf{k}_i,\mathbf{k}_f) = -\frac{m}{2\pi\hbar^2}\int e^{i(\mathbf{k}_i-\mathbf{k}_f)\cdot\mathbf{r}}v(\mathbf{r})d\mathbf{r}\,. \quad (2)$$

We show in Fig. 1 the exact $|f_e(\theta)|$ and $|f_p(\theta)|$ for electrons and positrons, respectively, at 100 eV, plotted as a function of the scattering angle θ between $\mathbf{k}_i$ and $\mathbf{k}_f$. The scattering factors are calculated from bulk fcc Cu potentials using the self-consistent, fully linearized, augmented plane wave method and taking only the spherical part of the potential (i.e., the muffin-tin approximation). The scatterer's charge is different, $+e$ for positron and $-e$ for electron, and the exchange-correlation potential is set to zero for positron diffraction. The positron's scattering factor $|f_p(\theta)|$ falls off smoothly from $\theta=0°$ to 180°, similar to the behavior of the Born differential cross section, while the electron's scattering factor $|f_e(\theta)|$ has cusps at 80° and 145° and rises sharply at 110° and 180°. We show in the inset of Fig. 1 the exact $|f_e(\pi)|$ (dotted line) and $|f_p(\pi)|$ (solid line) calculated from Eq. (1), as well as $|f_B(\pi)|$ (dashed line) calculated from Eq. (2). The Born approximation $|f_B(\pi)|$ for electrons and positrons is indistinguishable on the scale in Fig. 1. The positron's exact scattering factor at π is weaker in the energy range shown than its Born approximation value —they have a similarly smooth decay with energy —while the electron's exact scattering factor behaves

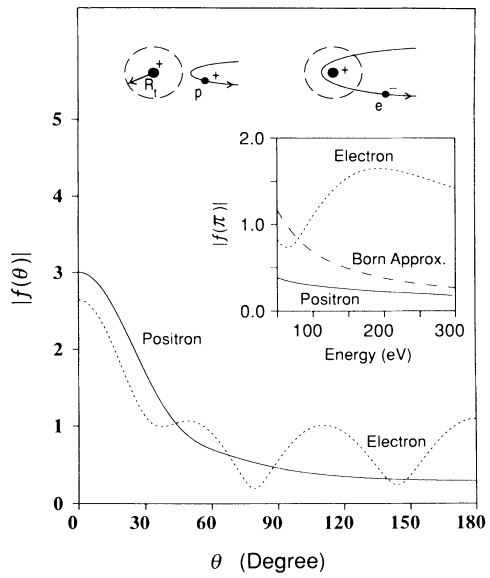

FIG. 1. Comparison of electron, positron, and Born approximation differential scattering factors of Cu.

drastically differently as it rises through a strong resonance at $E \approx 190$ eV. An important consequence of the near-Born behavior of $|f_p(\pi)|$ is that at scattering angles near π, the momentum transfer, $q = |\mathbf{k}_i - \mathbf{k}_f| = 2k \sin \frac{1}{2}\theta$, is large. This implies, from the integral of Eq. (2), that $f_p(q \approx 2k)$ is sensitive only to the small-r region of $v(r)$, a region that is dominated by the electrostatic Coulomb potential. This explains why the backscattered LEPD I-V spectra are rather insensitive to the exact form of the exchange-correlation potential, a fact reported in the early work of Jona *et al.* [18] and later again in the work of Weiss *et al.* [19]. For electrons, $|f_e(\pi)|$ is sensitive to all regions of $v(r)$ because of the higher-order terms in the expansion of Eq. (1). The physical consequence is that LEED I-V spectra are much more sensitive to the form of the exchange-correlation potential [16].

For positron diffraction, the exclusion principle is unimportant for its final-state distribution in solids [10]. This results in a larger inelastic damping for positrons than electrons at energies below 100 eV. At 100 eV or higher, a positron's inelastic damping is about the same as that of an electron's. The combination of weak elastic scattering and strong inelastic damping makes LEPD holography particularly attractive, as we demonstrate with an example: Cu(001)-$p(2\times2)$Se, in which the Se

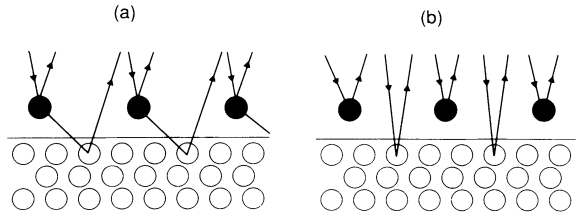

FIG. 2. Schematic diagrams of holographic LEED or LEPD: (a) Fractional-order scattering paths to be included; (b) integral-order paths to be excluded.

atoms are placed at 1.8 Å above fourfold hollow sites of the top-layer Cu atoms. The principles of local holography require considering scattering paths in which the adatom acts as a beam splitter for the reference and scattered waves. This condition is not satisfied for the integral-order spots where the strongest interference terms arise from backscattered waves from *different* layers, i.e.,

$$I_N(\mathbf{k}_f,\mathbf{k}_i) \propto |f_o^-(\hat{\mathbf{k}}_f\cdot\hat{\mathbf{k}}_i) + f_s^-(\hat{\mathbf{k}}_f\cdot\hat{\mathbf{k}}_i)e^{i(\mathbf{k}_i-\mathbf{k}_f)\cdot\mathbf{d}_1} + f_s^-(\hat{\mathbf{k}}_f\cdot\hat{\mathbf{k}}_i)e^{i(\mathbf{k}_i-\mathbf{k}_f)\cdot\mathbf{d}_2} + \cdots|^2, \quad (3)$$

where f_o^- and f_s^- are the scattering factors of the overlayer and substrate atoms, respectively, and $\mathbf{d}_1$, $\mathbf{d}_2$, etc., are vectors from the origin (taken to be at an adatom's nucleus) to substrate atoms in layers 1, 2, etc. [see Fig. 2(b)]. A Fourier integral of $I_N(\mathbf{k}_f,\mathbf{k}_i)$ with respect to $s_\perp = (\mathbf{k}_i - \mathbf{k}_f)_\perp$ yields peaks at distances $d_{1\perp}$, $d_{2\perp}$, etc., as well as at object-wave interference distances $(\mathbf{d}_1 - \mathbf{d}_2)_\perp$, $(\mathbf{d}_1 - \mathbf{d}_3)_\perp$, $(\mathbf{d}_2 - \mathbf{d}_3)_\perp$, etc. The situation is like using a meter stick to measure the distances of atoms $\mathbf{d}_i$, but the origin of the meter stick is at unknown positions $\mathbf{d}_j$. The presence of object-wave interference peaks [20] (i.e., artifacts) occurs because the condition that the reference wave is large compared to the object wave is not satisfied for I_N since an adatom's scattering factor is usually smaller than that of the substrate atoms, i.e., $|f_o^-| < |f_s^-|$. In addition, there are artifacts generated by multiple scattering [5–8]. Therefore, direct inversion of LEED or LEPD integral-order I-V spectra, as proposed in previous studies [11], is not a useful approach.

To invert LEED or LEPD intensity spectra, we need to consider exclusively those scattering paths which contain at least one scattering event at the adatom. These are exactly electrons collected at the fractional-order spots, whose leading interference terms are given by [5]

$$I_{N/2}(\mathbf{k}_f,\mathbf{k}_i) \propto \left| f_o^-(\hat{\mathbf{k}}_f\cdot\hat{\mathbf{k}}_i) + f_o^+(\hat{\mathbf{k}}_f\cdot -\hat{\mathbf{R}}_a)f_s^-(-\hat{\mathbf{R}}_a\cdot\hat{\mathbf{k}}_i)\frac{e^{ikR_a}}{R_a}e^{i\mathbf{k}_i\cdot\mathbf{R}_a} + f_s^-(\hat{\mathbf{k}}_f\cdot\hat{\mathbf{R}}_a)f_o^+(\hat{\mathbf{R}}_a\cdot\hat{\mathbf{k}}_i)\frac{e^{ikR_a}}{R_a}e^{-i\mathbf{k}_f\cdot\mathbf{R}_a} + \cdots \right|^2, \quad (4)$$

The first term in Eq. (4) may be viewed as a reference wave while the second and third terms are the single-scattering object waves from an atom at $\mathbf{R}_a$. The third term in Eq. (4), see Fig. 2(a), is identical to the single-scattering image term in photoemission holography if one replaces f_o^+ by an emission amplitude of the adatom. The second term represents a scattering path in which the particle propagates to a substrate atom, is backscattered by it via f_s^-, and is then forward scattered by an adatom into the detector. This term is also present in holographic diffuse LEED, and we have

shown how its effect may be eliminated by multiple-energy phase summation [5].

The effects of multiple scattering are also eliminated in the energy phase summation because a multiple-scattering path length—e.g., $\rho_\beta = R_\beta + |\mathbf{R}_\alpha - \mathbf{R}_\beta|$, which corresponds to an incident particle being scattered by an adatom at the origin, propagating to and being scattered by an atom at $\mathbf{R}_\beta$, followed by a scattering at $\mathbf{R}_\alpha$ before entering the detector—is normally longer than the direct distance from the origin to an atom at $\mathbf{R}_\alpha$ [8,21]. Similarly, object-wave interference artifacts formed by atoms $\mathbf{R}_\alpha$ and $\mathbf{R}_\beta$ are eliminated because the lengths $R_\alpha - R_\beta$ and $|\mathbf{R}_\alpha - \mathbf{R}_\beta|$ are unequal.

However, as opposed to photoemission holography and diffuse low-energy electron holography, a difficulty specific to holographic LEED or LEPD is that only discrete points in $\hat{\mathbf{k}}$ space are sampled [22]. These points are given by

$$\mathbf{k}_{f\parallel} = \mathbf{k}_{i\parallel} + \mathbf{g}\,, \tag{5}$$

where $\mathbf{g}$ is a two-dimensional reciprocal-lattice vector of the overlayer system. For the Cu(001)-$p(2\times2)$Se system, the reciprocal spots are shown in Fig. 3. We can sample fractional-order I-V spectra in the entire $\hat{\mathbf{k}}$ space by varying $\mathbf{k}_{i\parallel}$ over a mesh of directions. Two easy alternatives are present: The first choice is to use all the fractional-order spots (crosses and dots in Fig. 3) and vary $\mathbf{k}_i$ such that its projection in the g_x-g_y plane falls inside the small square whose corners are the (00), $(\frac{1}{2}0)$, $(\frac{1}{2}\frac{1}{2})$, and $(0\frac{1}{2})$ spots. Note that k_{ix} and k_{iy} are both negative. At 100 eV, the $(\frac{1}{2}0)$ beam is 13.9° from the normal. Using a mesh point with $\Delta\theta = 7°$, we need four $\mathbf{k}_i$ directions for the fractional-order spots to span the entire $\hat{\mathbf{k}}$ space [23]. With this choice, the intensities sampled at the integral-order spots are replaced by interpolative values obtained from those of nearby fractional-order spots [22]. The second choice, which is the one used in the example, is to select only the $c(2\times2)$ fractional-order spots (i.e., the dots in Fig. 3). In this case, the variations

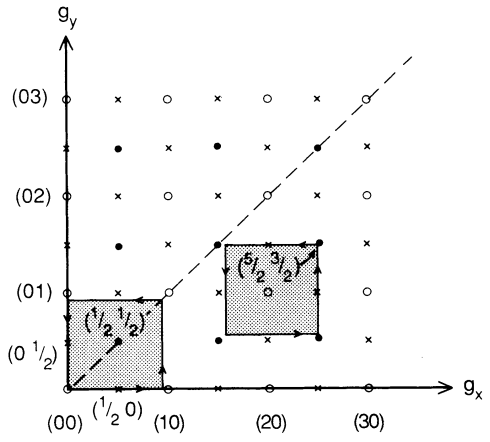

FIG. 3. Fractional-order spots which span the $\hat{\mathbf{k}}$ space as $\hat{\mathbf{k}}_{i\parallel}$ is varied.

of $\mathbf{k}_{i\parallel}$ will fall within the larger square whose corners are the (00), (10), (11), and (01) spots. A total of sixteen incident angles are needed but no intensity interpolation is necessary because, in this case, the integral-order spots as well as two-thirds of the fractional-order spots are discarded. The Cu(001)-$p(2\times2)$Se system has C_{4v} symmetry (as can be determined from the spot pattern at normal incidence); hence only those fractional-order spots in the one-eighth sector bounded by $g_x \geq g_y$ are used and a C_{4v} symmetry operation is applied to $I_{N/2}(\mathbf{k}_f, \mathbf{k}_i)$ to generate the complete 2π azimuthal range. In Fig. 3, we show the area spanned by one of the fractional spots, the $(\frac{5}{2}, \frac{3}{2})$ spot, as $\mathbf{k}_{i\parallel}$ is varied.

To generate the holograms, we calculated LEED and LEPD I-V curves using a standard multiple-scattering method developed for LEED [9] and the same dynamical inputs of phase shifts, inelastic damping, inner potential, vibrational amplitudes, etc., as those used in earlier dynamical LEED [24] and LEPD calculations [16–19]. The multiple-energy holographic transformation was done via the formula [6,7,25]

$$\phi(\mathbf{R}) = \sum_{n=1}^{N} e^{-ik_n R} \int \frac{\chi(k_n\hat{\mathbf{k}}) e^{ik_n\hat{\mathbf{k}}\cdot\mathbf{R}}}{\cos\theta} dk_{n,x}\, dk_{n,y}\,, \tag{6}$$

where $\chi(k_n\hat{\mathbf{k}})$ was a normalized intensity given by $\chi(k_n\hat{\mathbf{k}}) = I(k_n\hat{\mathbf{k}}_i, k_n\hat{\mathbf{k}}_f)/I_A(k_n\hat{\mathbf{k}}_i, k_n\hat{\mathbf{k}}_f) - 1$. The average function $I_A(k_n\hat{\mathbf{k}}_i, k_n\hat{\mathbf{k}}_f)$ was obtained by a seven-point averaging of $I(k_n\hat{\mathbf{k}}_i, k_n\hat{\mathbf{k}}_f)$. In the wave-number sum, a uniform grid of $\Delta k = 0.28$ Å^{-1} was used and the lowest electron or positron energy was 114 eV.

The reconstructed images, given by $\mu(\mathbf{R}) = |R\phi(\mathbf{R})|^2$, are shown in Fig. 4, viewed through a plane 1.8 Å below the Se layer. This plane passes through the nuclei of the topmost Cu atoms. The images shown, from left to right, are reconstructed by using increasingly more energies. For electrons (top panels), strong artifacts appear at nonatomic positions with two energies. As more energies are added via Eq. (6), the images at the atomic positions grow brighter while the intensities of artifacts become dimmer. With five energies, the images, at least for the four nearest-neighbor atoms, are sharply formed, although one can still detect (weak) artifacts approximately midway between the farther atoms. By contrast, using the same energies with positrons, the atom images are already formed at approximately the correct positions with only two energies. With increasing number of energies, the atomic positions marked by the images become more accurate while the intensities of the artifacts become weaker. Using only five energies in the range 114 eV $\leq E \leq$ 166 eV, the images for the first twelve neighbors are sharply formed, and the view is essentially free from serious artifacts. These images provide a direct view of the surface structure. Each circle in Fig. 4 has a diameter of 1.1 Å and its center marks the correct atomic position. The images from positron holography are shifted by less than 0.1 Å for the nearest-neighbor atoms and by ~0.3 Å for the next shell of atoms [3].

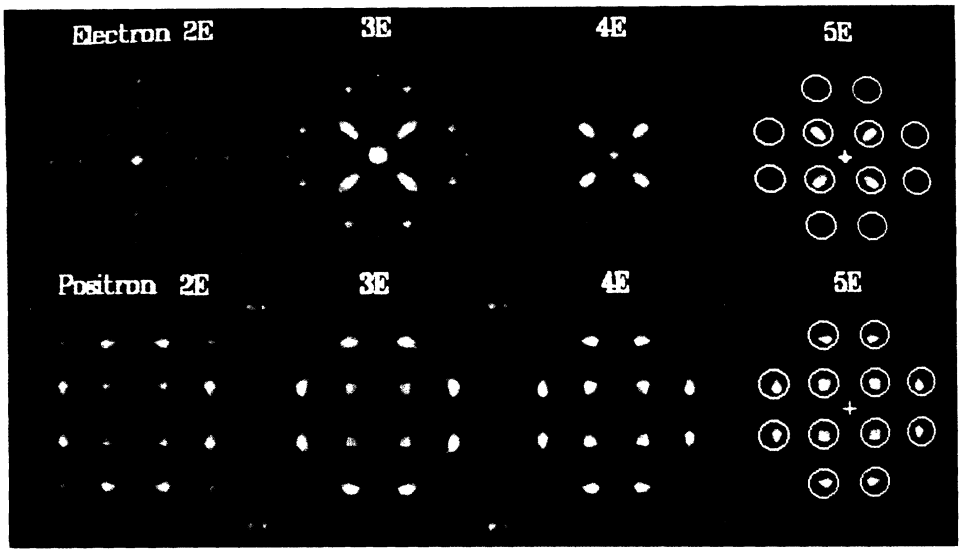

FIG. 4. Atom images from holographic reconstruction for electrons (upper panels) and positrons (lower panels) as more energies are added.

It is apparent that the complementary nature between imaging and diffraction methods makes their combination a most promising approach. Using essentially the same data set, imaging offers a three-dimensional view of the geometric arrangement with approximate atom positions while quantitative diffraction methods may be used to determine more accurately the bond lengths and angles. The obstacle of having to deal with massive amounts of trail geometries is eliminated in this combination. Positron holography has an additional advantage due to the weak scattering of positrons in solids which leads to a tremendous saving in data acquisition. Finally, we point out that such holographic reconstruction from diffraction patterns produces the statistically averaged local configuration of atoms around the adsorbate atoms.

This work is supported in part by the U.S. Department of Energy under Grant No. DE-FG02-84ER 45076.

[1] A. Szoeke, in *Short Wavelength Coherent Radiation: Generation and Applications*, edited by D. T. Attwood and J. Boker, AIP Conf. Proc. No. 147 (AIP, New York, 1986).
[2] J. J. Barton, Phys. Rev. Lett. **61**, 1356 (1988).
[3] S. Y. Tong, C. M. Wei, T. C. Zhao, H. Huang, and Hua Li, Phys. Rev. Lett. **66**, 60 (1991).
[4] D. K. Saldin and P. L. de Andres, Phys. Rev. Lett. **64**, 1270 (1990).
[5] C. M. Wei and S. Y. Tong, Surf. Sci. Lett. **274**, L577 (1992).
[6] S. Y. Tong, Hua Li, and H. Huang, Phys. Rev. Lett. **67**, 3102 (1991).
[7] J. J. Barton, Phys. Rev. Lett. **67**, 3106 (1991).
[8] S. Y. Tong, H. Huang, and C. M. Wei, Phys. Rev. B **46**, 2452 (1992).
[9] M. A. Van Hove and S. Y. Tong, *Surface Crystallography by LEED* (Springer, Berlin, Heidelberg, 1979).
[10] K. F. Canter, C. B. Duke, and A. P. Mills, in *Chemistry and Physics of Solid Surfaces VIII*, edited by R. Vanselow and R. Howe (Springer, Berlin, 1990).
[11] D. L. Adams and U. Landman, Phys. Rev. B **15**, 3775 (1977).
[12] I. J. Rosenberg, A. H. Weiss, and K. F. Canter, Phys. Rev. Lett. **44**, 1139 (1980).
[13] A. P. Mills, Jr., Appl. Phys. **23**, 189 (1980).
[14] R. Feder, Solid State Commun. **34**, 541 (1980).
[15] M. N. Read, D. N. Lowy, Surf. Sci. **107**, L313 (1981).
[16] C. B. Duke and D. L. Lessor, Surf. Sci. **225**, 81 (1990).
[17] D. L. Lessor, C. B. Duke, X. M. Chen, G. R. Brandes, K. F. Canter, and W. K. Ford (to be published).
[18] F. Jona, D. W. Jepsen, P. M. Marcus, I. J. Rosenberg, A. H. Weiss, and K. F. Canter, Solid State Commun. **36**, 947 (1980).
[19] A. H. Weiss, I. J. Rosenberg, K. F. Canter, C. B. Duke, and A. Paton, Phys. Rev. B **27**, 867 (1983).
[20] S. Thevuthasan, G. S. Herman, A. P. Kaduwela, R. S. Saiki, Y. J. Kim, W. Niemezura, M. Burger, and C. S. Fadley, Phys. Rev. Lett. **67**, 469 (1991).
[21] An exception is if $\mathbf{R}_\alpha$ and $\mathbf{R}_\beta$ are in a straight line with the adatom. In this case, both single- and double-scattering terms form an image at $\mathbf{R}_\alpha$.
[22] M. A. Mendez, C. Gluck, and K. Heinz, J. Phys. C **4**, 999 (1992).
[23] A few points near the origin may be blocked by the shadow of the electron gun. The intensities at these points may be obtained by interpolation.
[24] M. A. Van Hove and S. Y. Tong, J. Vac. Sci. Technol. **12**, 231 (1975).
[25] S. Y. Tong, Hua Li, and H. Huang, Phys. Rev. B **46**, 4155 (1992).

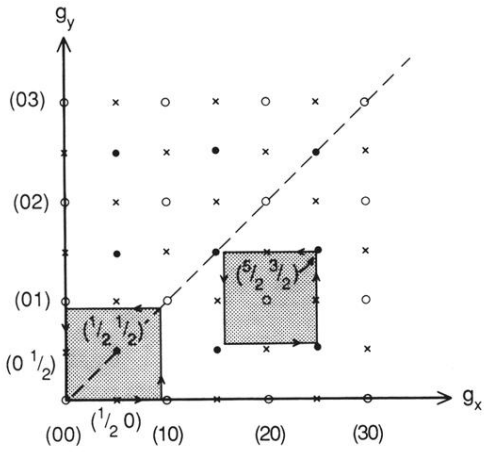

FIG. 3. Fractional-order spots which span the $\hat{\mathbf{k}}$ space as $\hat{\mathbf{k}}_{i\parallel}$ is varied.

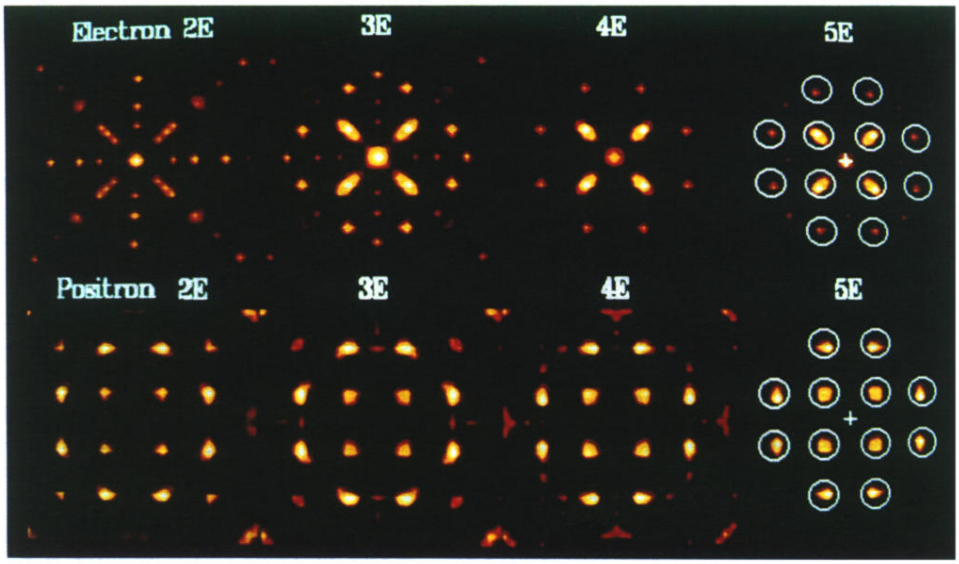

FIG. 4. Atom images from holographic reconstruction for electrons (upper panels) and positrons (lower panels) as more energies are added.